Aerodynamic Interference during Sabot Discard

E. M. Schmidt* and D. D. Shear†
U.S. Army Armament Research and Development Command, Aberdeen Proving Ground, Md.

An experiment has been conducted to investigate trajectory disturbances originating during the discard of sabot components from gun-launched fin-stabilized projectiles. The motion of the projectile and separating sabot components is measured near the muzzle of a 60-mm gun using an orthogonal array of flash x-rays. The downrange motion of the projectile is measured in a ballistics range. Apparently anomalous yawing motion of the projectile is correlated with asymmetries in the sabot discard geometry. Since mechanical contact is not observed between the sabot and projectile once discard commences, the measured large-amplitude angular acceleration is ascribed to aerodynamic interference between the sabot and projectile flowfields. The alteration in projectile yawing motion is demonstrated to agree with downrange measurements and to produce a significant increase in round-to-round dispersion.

Nomenclature

A	= cross-sectional area of the projectile
$C_D, C_{L_\alpha}, C_{M_\alpha}$	= drag, lift, and moment coefficients
I_x, I_y	= axial and transverse moments of inertia of the projectile
l	= projectile body diameter
M	= Mach number
$T/2$	= half-period of yaw
X, Y, Z	= Cartesian coordinates, Fig. 3
α, β	= projectile angle of attack and sideslip, Fig. 3
ξ	= complex angle of yaw, $\beta + i\alpha$
ρ, p	= air density and pressure
σ	= standard deviation of point of impact

Introduction

THE primary design being considered for antiarmor kinetic-energy rounds is the saboted fin-stabilized projectile. The presence of the sabot leads to unique problems both in-bore and upon shot exit. Within the gun, consideration must be given to unsupported length of the projectile, fin interactions with the propellant bed, gas sealing between components, and excitation of internal degrees of freedom. At shot ejection, the sabot is discarded, generating a set of mechanical and gasdynamic effects which must be analyzed in order to minimize transverse impulses prior to entry into free flight. Aerodynamic interference between discarding sabot components and the projectile is thought to affect the resultant trajectory; however, to date, measurements have not been obtained to quantify this interference for actual kinetic-energy rounds. This paper presents the results of an experimental program conducted to examine sabot and projectile dynamics during the discard process. Observations of geometric asymmetry in the sabot discard pattern and associated behavior of the projectile are used to postuate the existence of strong aerodynamic interactions.

While aerodynamic interference between components of aircraft (e.g., wing/body, airframe/propulsion, and airframe/stores) has been extensively investigated,[1] similar interference associated with sabot discard from high speed projectiles has received limited attention.[2-4] Gallagher[2] presents an experimental investigation of projectile deviation from the desired aim point due to muzzle blast, sabot discard, and projectile asymmetry. Since he neglects any contribution due to gun tube/projectile interaction, the value he assigns to deviation due to muzzle blast is orders of magnitude greater than found in more recent investigations.[5,6] These show muzzle blast does not contribute significantly to trajectory deviation and that the actual source lies with gun tube or sabot discard interactions. Gallagher notes that the sabot components open symmetrically, but the center of gravity of the grouped components does not lie along the axis of the projectile. He assumes that there will be a momentum exchange between the sabot and projectile in relation to their masses and the magnitude of the center of gravity separation. However, due to the limitations of his apparatus, Gallagher could not define the magnitude of this deviation. He made no attempt to investigate the effects of aerodynamic interactions.

Conn[3] investigates the effect of aerodynamic interference between sabots and projectiles fired from a light gas gun. His measurements show that a conical projectile launched with a two-segment sabot has periods of pitch and yaw which depend upon the orientation of the sabot plane of separation. He uses oblique shock and Newtonian flow theory to analyze the pressure distribution on a cone at an arbitrary attitude relative to a symmetrically discarded two-segment sabot. The results of his analysis show that aerodynamic interference differentially increases the restoring moments acting on the cone, thereby shortening the periods of oscillation.

Glauz[4] uses oblique shock theory to analyze the side forces and moments generated on a fin-stabilized projectile due to a single sabot component flying in close proximity. He assumes that when it intercepts the projectile, the shock wave from the sabot is planar, does not reflect at the projectile, and is not influenced by the projectile viscous or inviscid flow field. In a sample calculation, Glauz predicts a significant alteration of the trajectory of a small-caliber flechette by this type of discard process; however, his calculated value of discard-induced angular velocity is an order of magnitude higher than actually measured.[7] This disagreement is due to both the simplistic nature of the model and the complex mutually interacting flows established during discard.

The present investigation was conducted to provide detailed information on the interference between sabot components and the projectile for actual kinetic energy round configurations. Measurements of sabot and projectile motion from the gun muzzle, through sabot discard, and into undisturbed free flight are presented. Observed large-amplitude

Presented as Paper 77-1142 at the AIAA Atmospheric Flight Mechanics Conference, Hollywood, Fla., Aug. 8-10, 1977; submitted Sept. 20, 1977; revision received Jan. 30, 1978.

Index categories: LV/M Dynamics and Control; LV/M Trajectories and Tracking Systems.

*Aerospace Engineer, Launch and Flight Division, Ballistic Research Laboratory. Member AIAA.

†Physical Science Technician, Launch and Flight Division, Ballistic Research Laboratory.

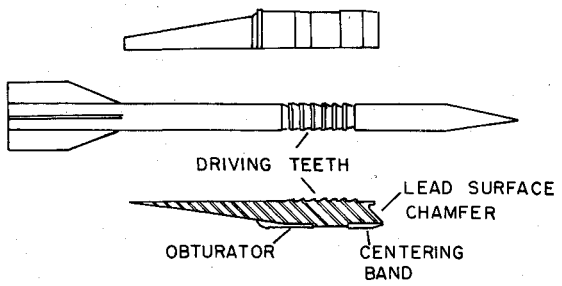

Fig. 1a Schematic of test projectile with two of the four sabot petals.

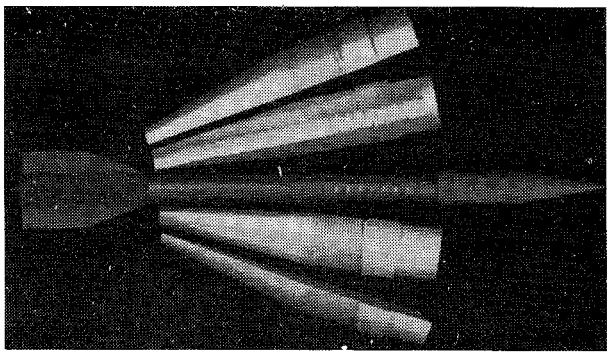

Fig. 1b Photograph of test projectile with four sabot petals.

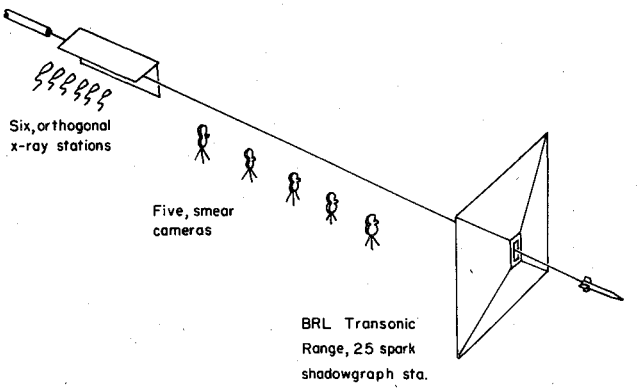

Fig. 2 Schematic of experimental apparatus.

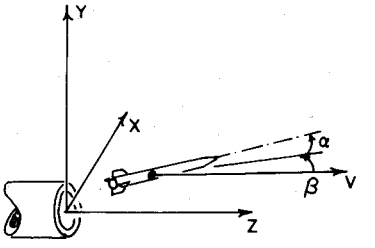

Fig. 3 Coordinate system.

projectile angular accelerations are shown to correlate with measured asymmetry in the sabot component discard geometry. Since mechanical reimpingement does not occur, the motion is ascribed to aerodynamic interference. A simplistic analysis of the interacting flow is used to estimate projectile loadings.

Data Acquisition and Test Procedure

The round tested is shown schematically in Fig. 1a and in the photographic layout of Fig. 1b. The projectile has a body diameter of 23 mm, a length of 423 mm, and is stabilized by four fins having a span of 56 mm. A four-segment sabot is employed to launch the projectile from a 60-mm gun. The sabot engages the projectile through a set of buttress threads. Additional in-bore support is achieved through friction drive generated on the rear ramped section of the sabot. The assembly is held together, centered in the tube, and sealed against propellant gas leakage by circumferential plastic and polycarbonate bands. These are discarded almost immediately upon separation from the gun tube. The launch velocity is 1310 m/s. Since the gun tube has a twist of rifling of one turn in 200 calibers of projectile travel, the initial free-flight roll rate is 110 rev/s.

A schematic of the test layout is shown in Fig. 2. Near-muzzle motion is monitored at six orthogonal x-ray stations located at 1.7-m intervals over the first 9.0 m of the trajectory. The x-ray photographs provide information on the sabot and projectile motion as the sabot is discarded. Downrange of the x-ray stations, five smear cameras set at 4.6-m intervals cover the final aerodynamic discard of the sabot components. At 35 m from the muzzle, the projectile enters the Ballistic Research Laboratory (BRL) Transonic Range while sabot components are intercepted on an armor plate shield at the range entrance. The range consists of an array of 25 orthogonal spark shadowgraph stations extending from 40 to 220 m forward of the weapon muzzle. The measured projectile motion is used for a number of purposes. First, it provides a basis for determination of projectile aerodynamic coefficients: $C_{L_\alpha} = 10.1$, $C_{M_\alpha} = -21.5$, $C_D = 0.46$. Second, the least-squares fit to the projectile yawing motion through the range is extrapolated back to the muzzle of the gun for comparison with x-ray measurements. The validity of this procedure will be discussed in the next section. Finally, the range data is used to define the round-to-round dispersion for the firing series.

To permit rapid quantitative reduction of the x-ray data, an in-situ calibration procedure is employed. A calibrated steel wire is surveyed into position along the line of fire prior to each shot. An x-ray photograph of the wire is obtained for all stations. The wire is removed, and the round is fired. In this manner, a double exposure is obtained on each photograph. The projectile center of gravity location and axis of symmetry orientation are measured with respect to the calibration wire and fiducial beads strung along it. These measurements are corrected for wire catenary, viewing plane of the x-ray film, and c.g. trajectory.[7] Final presentation of the data is made in a coordinate system identical to that used in the Transonic Range reduction (Fig. 3). In this system, the angle of sideslip β (measured positive as shown) is the angle between the projectile velocity vector and the plane containing the projectile axis and a vector parallel to the Y axis. The angle of attack α is the angle between the normal projection of the velocity vector into the aforementioned plane and the projectile axis.

Experimental Results

The Transonic Range data gives a direct indication of the impact of sabot discard interactions upon the dynamics of the ten rounds fired in this series (Fig. 4). The plot shows the distribution in yaw angle at the weapon muzzle predicted by rearward extrapolation of the least-squares fit to the measured projectile motion. Two sets of data are presented: the 60-mm saboted test projectile, and a 155-mm full-bore, spin-stabilized projectile, M483. In each case, the distance from the weapon muzzle to the first range station was roughly 40 m. The purpose of the figure is twofold: first, to demonstrate the validity of extrapolating the range data toward the muzzle, and second, to indicate the effect of sabot discard interference.

The Transonic Range measures the oscillation of the projectile in response to an initial perturbation and aerodynamic loadings. The latter information is used to define the aerodynamic coefficients. The former may be examined if the range data can be extrapolated back to the point in the projectile trajectory where the perturbation

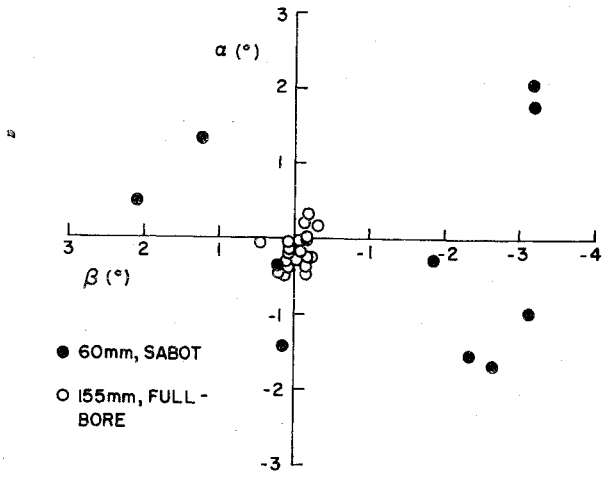

Fig. 4 Comparison of projectile yaw angle at the weapon muzzle predicted by rearward extrapolation of Transonic Range data.

occurs. For a spin-stabilized projectile, it is reasonable to assume that this perturbation should occur in the vicinity of the gun tube. Specifically, the initial free-flight dynamics of the round should correspond to the dynamic properties it had upon separation from the gun. In the bore, the projectile is mechanically constrained and can not reach yaw levels greatly in excess of 0.2 deg[8]; however, its angular velocity may be substantial. As it separates from the tube, mechanical disengagement and muzzle blast loadings may amplify the angular rate, but due to the short time over which these loads act,[6] the yaw level should not grow significantly. Thus, if the current extrapolation of the Transonic Range data is a valid technique, it will predict that a spin-stabilized round is launched with low yaw but finite angular velocity. Examination of the M483 data shows that this is indeed the case. The yaw level in the vicinity of the muzzle is less than 0.5 deg for all rounds tested, with the majority less than 0.25 deg; however, the angular rate at the muzzle was sufficient to produce first maximum yaw levels from 1 to 7 deg. Since the accuracy of the range measurement is roughly 0.2 deg, the extrapolation agrees to within the experimental accuracy with anticipated launch conditions. This agreement is taken to indicate the validity of extrapolating the yawing motion of the shell rearward a distance corresponding to roughly one cycle in its oscillatory motion.

Examining the extrapolated yaw level for the saboted projectile (Fig. 4) shows that the muzzle is not a point of minimum or even small yaw. This reflects the difference in launch perturbation between the full-bore and saboted round. Once the full-bore round penetrates the muzzle blast, it is in undisturbed free flight. However, the saboted round must in addition fly through a region disturbed by the discarding sabot components. During this relatively long duration transition, both the angle of attack and angular velocity may be altered from the separation values. The range data indicates the response of the round to the total launch impulse, i.e., both in-bore and sabot discard related; thus, the extrapolation would not be expected to produce closure or low yaw at the muzzle unless the sabot discard environment was identical to undisturbed free flight. The fact that the yaw levels are not minimum indicates that during sabot discard conditions are significantly different from free flight.

The x-ray data provides information on the nature of this initial flight environment (Fig. 5). This sequence of photographs is compiled from the vertical plates of the six x-ray stations exposed during a single firing. The film plane is parallel to the ground and above the flight path; therefore, the view is that of an observer situated above the projectile watching it fly downrange beneath him. The stations are located over the first 9.0 m of the trajectory. The sabot

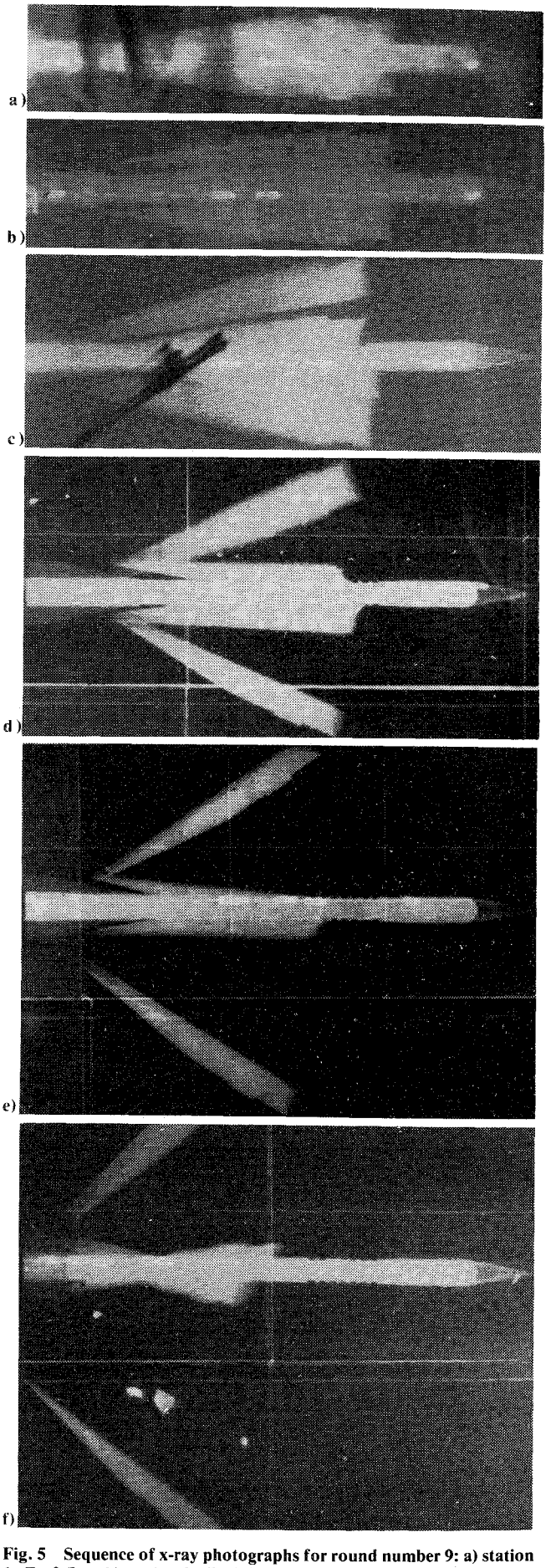

Fig. 5 Sequence of x-ray photographs for round number 9: a) station 1, $Z = 0.7$ m; b) station 2, $Z = 2.3$ m; c) station 3, $Z = 4.0$ m; d) station 4, $Z = 5.8$ m; e) station 5, $Z = 7.4$ m; f) station 6, $Z = 9.0$ m.

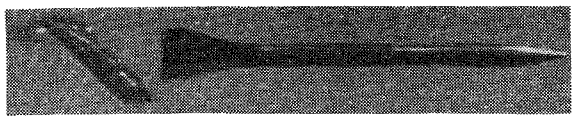

Fig. 6 Smear photograph for round number 9, $Z = 13.7$ m.

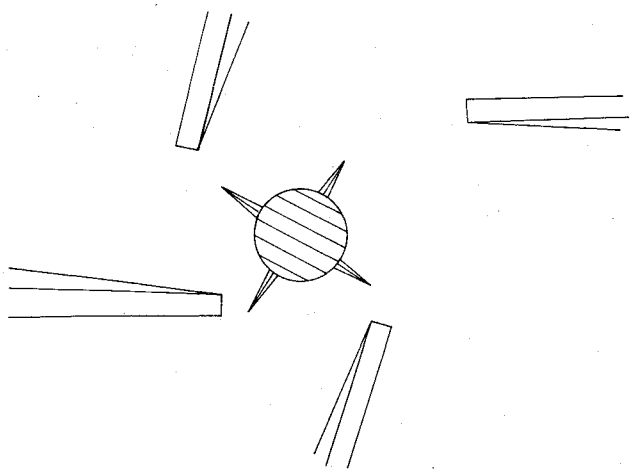

Fig. 7 Sabot petal geometry relative to projectile for round 9, station 5, $Z = 7.4$ m.

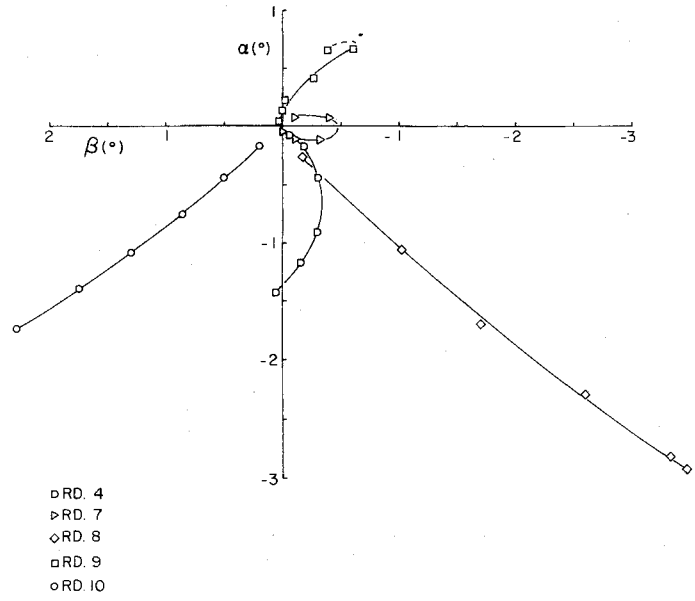

Fig. 8 Variation of yaw angle through x-ray field of view.

components remain in close proximity to the projectile through the x-ray range; however, by the first smear camera, located 13.7 m forward of the gun (see Fig. 6), they have achieved sufficient lateral and rearward separation to preclude communication with the projectile. It is estimated that interaction between the sabot and projectile flowfields terminates at approximately 11.0 m from the muzzle.

Examination of the discard sequence reveals some interesting features (Fig. 5). At the first x-ray station, the only observable motion of the sabot is the shedding of plastic centering and obturating bands. At 2.3 m, the sabot components have moved laterally away from the projectile but show little pitch or yaw. This initial motion is thought to be due to a combination of elastic decompression at separation and the tangential/angular velocity due to the launch roll rate (110 rev/s), and is carried through the muzzle blast with very little amplification. The round penetrates the muzzle blast at approximately 1.5 m. Once out of the blast, strong aerodynamic loadings will be generated on the sabot components (launch Mach number = 3.91). The effect of which is not seen at 2.3 m, but by the third x-ray station, $Z = 4.0$ m, the components are pitching away from the projectile due to loads on the front chamfer of the sabot. Subsequent x-ray photographs show the continuation of this pitching motion and resultant lifting away from the projectile. Due to the high drag of the light sabot components at this attitude, they decelerate more rapidly than the projectile and fall behind relative to the flight body.

In the final two photographs of this sequence, an asymmetry in the discard geometry is apparent. The sabot petal on the left side (upper component in picture) is closer to the projectile than is the right-hand petal. A construction of the sabot pattern at $Z = 7.4$ m clarifies this asymmetry (Fig. 7). The view is from the rear along the axis of the projectile at a cut taken through the aft of the sabot petals (Fig. 5e). While the photograph appears to show possible contact with the fins, the construction shows that this is not the case. The upper and lower sabot components are symmetrically arranged with respect to the projectile; however, this is not true of the lateral components. The left component is extremely close to a fin surface, suggesting the probability of strong interaction.

The measured yawing motion gives an indication of the magnitude of aerodynamic interference. A plot of the projectile angles of attack and sideslip for five typical firings is presented in Fig. 8. Each data point is a separate measurement from an orthogonal x-ray station. The data is presented as if one were viewing the projectile from the rear; effectively, the coordinate axes could be thought of as representing the fins while the data point corresponds to the attitude of the projectile nose relative to them. A variety of yawing motions are observed. All start with a magnitude of yaw near the muzzle which is quite small, roughly 0.1 deg, consistent with anticipated in-bore values.[8] These contrast with the range extrapolations given in Fig. 4, indicating the error in attempting to carry the Transonic Range data fit through the sabot discard region. The angular velocities at the muzzle are significant and have fairly random orientations. Some rounds show a monotonically increasing yaw, while others have yaw which first increases to a maximum value quite close to the gun and then begins to decrease. The fact that this is not normal free-flight yawing motion can be drawn from examination of the Transonic Range data, Table 1.

The range data show that, in undisturbed free flight, the distance traveled by the projectile between successive minima in the absolute value of yaw, the half-period of yaw $T/2$, is fairly constant and has an average value of 39.2 m. The projectile would attain a maximum value of yaw halfway between the minima; thus, the distance from a minimum to a maximum value of yaw would be 19.6 m. Assuming a

Table 1 Summary of projectile yawing motion from Transonic Range data

Round no.	First max. yaw, deg	$Z_{1st\ max.}$, m	$T/2$, half-period of yaw, m
1	3.31	27.5	40.8
2	6.52	24.0	40.6
3	7.78	26.5	39.8
4	1.74	16.0	36.3
5	3.68	22.3	37.0
6	3.02	11.3	38.3
7	4.29	29.0	38.7
8	4.45	10.5	39.8
9	5.59	28.9	40.0
10	8.07	23.8	40.4

projectile left the weapon muzzle and immediately began to experience free-flight aerodynamic loads, its yaw level would continually increase for 19.6 m. The x-ray data in Fig. 8 show this is not necessarily the case. Two of the rounds tested show yaw levels which reach a maximum at 7 m from the muzzle and begin to decrease, implying a reduction in the period of yaw by a factor of 2.8. The half-period of yaw of a statically stable projectile may be approximated as

$$T/2=\pi(2I_y/C_{M_\alpha}\rho Al)^{1/2} \quad (1)$$

which, for the test projectile, yields $T/2=37.6$ m – a value well bounded by those tabulated. Examination of Eq. (1) shows that a reduction in the half-period by a factor of 2.8 is equivalent to an increase in the aerodynamic moment by a factor of 8 over that in the free field. This substantial value of aerodynamic loading reflects the severity of the discard interactions.

Further indication of these effects may be seen in the distribution of first maximum yaw location relative to the gun, covering a range of 10.5 to 29.0 m forward of the muzzle. The two extremum rounds, round 7 and round 8, provide insight into the alterations in projectile dynamics which produce this spread of $Z_{1\text{st max}}$. The yawing motion of round 7 (see Fig. 8) reaches a maximum within the field of view of the x-rays and approaches a minimum yaw point near the last station, $Z_6=9.6$ m $\cong T/8$. Contrasting with this behavior, the yawing motion of round 8 monotonically increases over the same distance; however, its angular velocity – indicated by the spacing between data points – decreases until at the last station it approaches a maximum yaw point. Considering these changes to be phase shifts from the nominal or interference-free motions, the oscillation of round 7 has a 135-deg advance in phase as it passes the last x-ray station. The next maximum of yaw should occur at $Z=3T/8=29.4$ m, which is approximately the distance obtained from Table 1. Similarly, round 8 displays a 45-deg advance in phase as it passes x-ray station 6, yielding a first maximum yaw point at $Z=T/8=9.8$ m. Again, this is approximately the first maximum yaw location obtained from the Transonic Range extrapolation in Table 1 and typifies the agreement between the two means of data acquisition (Fig. 9). Both sets of data agree in predicting the magnitude and rate of change of yaw at the point where aerodynamic interactions are diminishing toward the free-flight conditions. Similar comparisons may be made between other rounds in this sequence confirming the accuracy of the experimental technique.

The origin of the aerodynamic loadings which generate the observed projectile motion may be investigated by comparing the x-ray photographs for round 9 (Fig. 5) with the data presented in Fig. 8. In Figs. 5d-5f, the left-hand sabot petal is closer to the projectile than is the petal on the right. Simultaneously, symmetry is maintained in the vertical plane (Fig. 7). Such a sabot petal geometry should result in unbalanced aerodynamic loads upon the projectile. The shock from the left-hand petal would impinge further up on the body than that from the right-hand petal. The result would be an unbalanced force on the aft of the projectile directed to the right. This force generates a moment which causes the projectile nose to yaw left, as is measured in the x-ray data (Fig. 8). The angular acceleration at station 5 is obtained by differencing the x-ray measurements: $\ddot{\beta}_5=0.72\times10^4$ rad/s^2. A relatively simple model of the interference flowfield may be postulated for the geometry of round 9.

Assume that symmetry exists in the vertical plane, i.e., the upper and lower sabot petals are equidistant from, and identically inclined with respect to, the projectile. Only the asymmetries in the horizontal plane will be considered. The sabot components are approximated as two semi-infinite wedges of equal half-angle, 30-deg (see Fig. 10) – an average of the inclination of the cylindrical and ramp sections. The tip of each wedge section is located at the leading edge of the sabot petal in Fig. 5e. The weak oblique shocks which are generated as the freestream is deflected through the wedge angle then impinge on the body at locations separated by roughly two body diameters. The Mach number[9] behind the oblique shocks is $M_2=1.80$. The flow is assumed to turn back to an axial direction when the shocks intersect the body; however, at $M_2=1.80$, the flow deflection angle exceeds that possible with an attached shock. As such, a Mach reflection occurs and the pressure along the body is taken to be uniform and equal to the static pressure behind a normal shock wave with $M_1=3.91$, or $p_2/p_1=17.7$. Neglecting crossflow around the body, the resulting side force is 1878 N and produces an angular acceleration of 0.81×10^4 rad/s^2. The agreement between this estimate and the measured value is good, but the simplicity of the aerodynamic model and the inaccuracies associated with differencing experimental data lead to the conclusion that such correspondence is largely fortuitous. Rather than being put forward as an exact treatment of the problem, this calculation is included to support the conclusion that the observed angular accelerations of the projectile are due to sabot discard aerodynamic interference.

Estimated Trajectory Perturbation

The impact of interference upon the projectile trajectory can be estimated by considering the change in effective launch angular rate of the projectile due to the discard process. The x-ray data provide information on the actual angular rate of the projectile at separation from the gun tube. Using a differencing formula ξ_2, the angular rate of the projectile at station 2, $Z=2.3$ m, may be computed. This rate is equivalent to the lateral impulse transferred to the projectile during in-bore acceleration and passage of the blast. Since it has been demonstrated that the Transonic Range data fit may not be

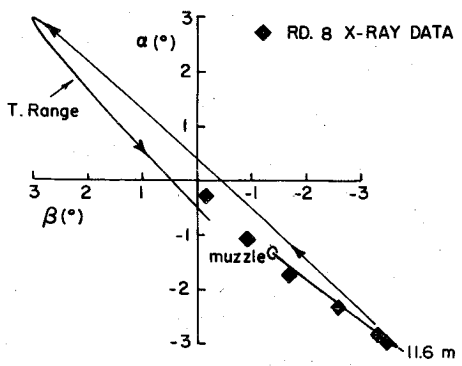

Fig. 9 Comparison of x-ray measurements of yaw angle variation with extrapolation of Transonic Range data.

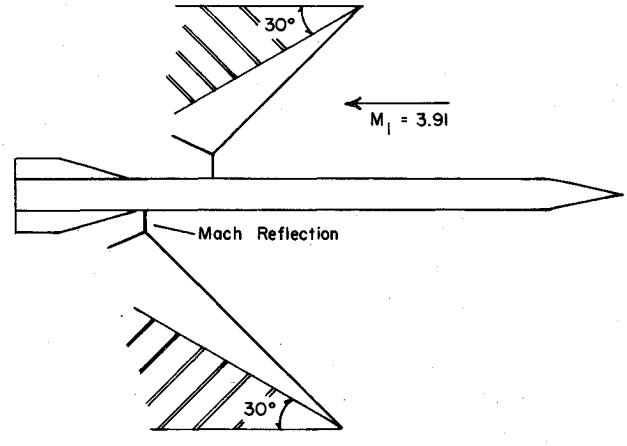

Fig. 10 Shematic of flowfield approximation for round 9, station 5, $Z=7.4$ m.

Table 2 Comparison of angular velocities

Round no.	$\lvert\dot{\xi}_2\rvert$, deg/s	$\lvert\dot{\xi}_0\rvert$, deg/s	$\lvert\dot{\xi}_2\rvert - \lvert\dot{\xi}_0\rvert$, deg/s
1	no x-ray	354	...
2	365	686	321
3	239	827	588
4	174	186	12
5	205	393	188
6	427	323	−104
7	98	459	361
8	818	481	−337
9	74	592	518
10	342	862	520

extrapolated back to the weapon muzzle with any accuracy, and since the termination of the interaction zone is not well defined, an effective "launch" angular velocity must be defined based on the level of first maximum yaw reached by the round. Neglecting spin and damping,

$$\dot{\xi}_0 = \xi_{1\text{st max}} (C_{M_\alpha} \rho V^2 lA/2I_y)^{1/2} \tag{2}$$

The rate given by Eq. (2) represents the cumulative angular impulse transferred to the projectile by in-bore, muzzle blast, and sabot discard loadings. Following this reasoning, the difference of these two rates should give the impulse due aerodynamic interference:

$$\Delta\dot{\xi} = \dot{\xi}_0 - \dot{\xi}_2 \tag{3}$$

These impulse parameters are compared in Table 2.

While the last column is a scalar rather than vector difference, it does indicate the relative magnitude of the impulse generated by aerodynamic interaction. Comparison of the last column with the second column shows that the aerodynamic interaction effect is equivalent to that due to in-bore and muzzle blast loadings. This has a significant effect upon accuracy. The impact distribution of the various rounds on-target are computed using two procedures: 1) extrapolation of x-ray station 2 dynamics downrange through use of the jump relations,[6] and 2) from measured projectile positions at the final Transonic Range station. These are presented in Fig. 11. Both of the procedures yield elliptical impact patterns with identical orientation of the principal axis; however, these are differences in the size of the patterns. As expected, the extrapolated x-ray data present the smallest pattern since they do not include the effect of aerodynamic interactions. The measured impact pattern is roughly 30% greater in area than is the extrapolated pattern. This difference indicates that the growth of dispersion due to aerodynamic interference between the sabot components and the projectile is significant in terms of the overall system accuracy.

An unresolved question is the origin of the asymmetries in the sabot discard pattern. It is likely that the interior ballistics and mechanical disengagement of the round have important input to the initial separation dynamics which drive the generation of sabot pattern asymmetry. Additionally, it has been conjectured that differential fracture of the front and rear bands could be a contributing factor. At present, it appears that the best solution to the problem of decreasing the effect of interference lies not in reducing asymmetry, but in providing for more rapid discard. Increasing the speed with which the sabot clears the projectile will decrease the aerodynamic impulse transferred due to asymmetries.

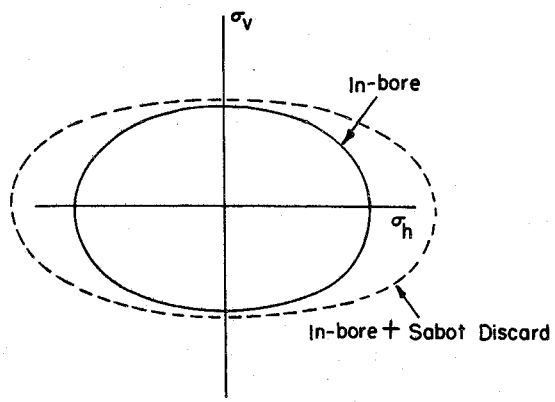

Fig. 11 Comparison of target impact patterns.

Conclusion

An experimental program is presented which defines the sabot discard and launch dynamics of a 60-mm fin-stabilized projectile. The resulting data indicate that aerodynamic interference occurs between the discarding sabot components and the projectile. A simple analysis of the magnitude of aerodynamic loadings that could be generated in the discard process indicates that the measured alterations of the projectile trajectory are well estimated. The impulse due to interaction is found to be of the same magnitude as the in-bore and muzzle blast impulse. Its effect is to increase the dispersion of the system significantly. To reduce the effect of aerodynamic interaction, it is advisable to implement rapid sabot discard, thereby decreasing the duration of impulse loadings.

References

[1] Sears, W.R. (ed.), "Aerodynamic Interference," AGARD, CP-71-71, Jan. 1971.

[2] Gallagher, W.J., "Elements which have Contributed to Dispersion in the 90/40 mm Projectile," Ballistic Research Laboratory, Aberdeen Proving Ground, Md., R1013, March 1957.

[3] Conn, H., "The Influence of Sabot Separation on the Yawing Motion of a Cone," Defense Research Establishment, Valcartier, Canada, TN 1849/70, June 1970.

[4] Glauz, W.D., "Estimation of Forces on a Flechette Resulting from a Shock Wave," Midwest Research Institute, Kansas City, Mo., R3451-E, May 1971.

[5] Gretler, W., "Intermediate Ballistics Investigations of Wing Stabilized Projectiles," Deutschen Versuchsanstaldt für Luft-und Raumfahrt, Aachen, West Germany, R67-92, Nov. 1967.

[6] Schmidt, E.M., Fansler, K.S., and Shear, D.D., "Trajectory Perturbations of Fin-Stabilized Projectiles due to Muzzle Blast," *Journal of Spacecraft and Rockets*, Vol. 14, June 1977, pp. 339-344.

[7] Schmidt, E.M. and Shear, D.D., "Launch Dynamics of a Single Flechette Round," Ballistic Research Laboratory, Aberdeen Proving Ground, Md., R1810, Aug. 1975.

[8] Gay, H., "Notes on the Yawing Motion of a Projectile in the Bore," Ballistic Research Laboratory, Aberdeen Proving Ground, Md., MR 2259, Jan. 1973.

[9] Ames Research Staff, "Equations, Tables, and Charts for Compressible Flow," NACA 1135, 1953.